Thermoviscoplastic modeling of the shearing process for mechanism-driven fine blanking of high manganese steel

Frank SCHWEINSHAUPT[1,a *], Martina MÜLLER[1,b], Tim HERRIG[1,c] and Thomas BERGS[1,2,d]

[1]Manufacturing Technology Institute – MTI of RWTH Aachen University, Campus-Boulevard 30, 52074 Aachen, Germany

[2]Fraunhofer Institute for Production Technology IPT, Steinbachstr. 17, 52074 Aachen, Germany

[a]f.schweinshaupt@mti.rwth-aachen.de, [b]m.mueller@mti.rwth-aachen.de, [c]t.herrig@mti.rwth-aachen.de, [d]t.bergs@mti.rwth-aachen.de

Keywords: Thermoviscoplastic Model, High Manganese Steel, Fine Blanking, Shearing

Abstract. The sheared surface hardening resulting during fine blanking of high manganese steel (HMnS) offers potential for increasing fatigue and wear resistance and thus for substituting heat treatment for tribologically stressed fine blanked parts. The stresses and temperatures occurring in the shear zone lead to interactions with the alloy design-dependent deformation mechanisms of HMnS, which influences the achievable sheared surface hardening as well as quality. In order to develop an alloy design for HMnS tailored to the shearing process to achieve high deformation mechanism-driven sheared surface hardening while maintaining high quality, knowledge of the stress state and temperature in the shear zone is required. This paper deals with thermoviscoplastic material modeling of HMnS X40MnCrAlV19-2 Low Yield (LY) for numerical analysis of the shearing process during fine blanking. For this purpose, stack compression tests were carried out with variation of temperature and strain rate. The flow curves derived from the compression tests were extrapolated to determine the parameters for a temperature- and strain rate-dependent flow curve model according to Hensel-Spittel using regression analysis. Based on a thermally coupled finite element (FE) model for fine blanking, various extrapolated flow curve parameters were analyzed numerically and compared with force and temperature measurements from experimental fine blanking tests. The Hensel-Spittel modeling derived from the combined Swift-Voce extrapolation showed a sufficiently accurate correspondence to the experimental results regarding the numerical blanking force and sheared surface temperature.

Introduction

The characteristics of fine blanking lead to a thermomechanically induced heat dissipation in the shear zone due to locally high strains during the shearing process, which is influenced by the process parameters. The dissipated heat accumulates in the shear zone and causes a significant temperature increase along the shearing path depending on the process parameter-influenced load spectrum [1]. During fine blanking of HMnS, the temperature development along the shearing path has a significant influence on the activation of the deformation mechanisms and thus on the resulting sheared surface hardening as well as quality [2]. Therefore, the development of an alloy designed for fine blanking of HMnS requires numerical modeling of the shearing process to analyze the process parameters with thermomechanical influence. Due to the locally high strains in the shear zone, modeling of the flow behavior with true strains φ significantly higher than one is required for a sufficiently accurate analysis of plastic flow during fine blanking. Consequently, adequate material characterization is essential to ensure reliable modeling results. For characterizing sheet metal materials, several mechanical test methods allow the determination of flow curves with higher true strains, which are for example comprehensively described in [3] or

Content from this work may be used under the terms of the Creative Commons Attribution 3.0 license. Any further distribution of this work must maintain attribution to the author(s) and the title of the work, journal citation and DOI. Published under license by Materials Research Forum LLC.

analyzed and compared in [4] regarding their accuracy. Plastic flow in the shear zone of the fine blanked sheet metal material occurs similar to bulk metal forming under a hydrostatic compressive stress state, which suggests that the stack compression test (SCT) is a suitable mechanical test method for determining flow curves with higher achievable true strains.

For SCTs, rectangular or rotationally symmetrical specimens are manufactured to stack the individual layers of the sheet metal material to be investigated. The occurring and inevitable friction at the upsetting plates in contact with the specimen surfaces requires a correction of the flow curve, especially at lower aspect ratios (stacked height h to diameter d or width b). Based on the elementary plasticity theory, the relationship between the normal stress occurring during a deformation and the friction-induced shear stress for a volumetric body can be described analytically under assumption of the Coulomb friction model and von Mises yield criterion [5]. This approach enables a friction correction of the flow curve and is also referred to as friction hill analysis due to the exponentially increasing stress progression from the edge of a cylindrical body to the center of the axis. Investigations by An et al. on SCT with low carbon steel showed that the influence of friction on the flow stress is reduced with a higher aspect ratio of h/b = 1.25 and corrected the flow curve using the friction hill analysis [6]. Hochholdinger et al. carried out temperature- and strain rate-dependent SCT to model the flow behavior for hot forming of 22MnB5 and determined a constant friction coefficient in an inverse numerical analysis for considering the influence of Coulomb friction on the flow curve [7]. Kraus et al. analyzed sheet metal specimens made of dual phase steel DP600 and cold rolled steel DC06 in a single layer compression test and showed a change of the Coulomb friction coefficient as well as the friction factor depending on the contact normal stress under both lubricated and dry contact conditions [8]. In a study by Kölüs et al., flow curves of cold rolled steel DC04 at different aspect ratios were determined using SCT and the influence of Coulomb friction on the flow curve was investigated based on the friction hill analysis [9]. With a larger aspect ratio of h/d = 1, the corrected flow curves for a constant assumed friction coefficient as well as a friction coefficient dependent on the contact normal stress showed an approximately comparable progression. For the numerical analysis of forming processes with higher true strains, an extrapolation of the experimentally determined flow curves is required to model the flow behavior. A large number of scientifically established strain hardening laws exist for extrapolation, which differ in their progression at higher true strains [10]. Lemoine et al. investigated various hardening laws for the extrapolation of experimentally determined flow curves for Advanced High Strength Steels (AHSS) and showed sufficiently accurate results in subsequent numerical forming simulations for the combined Swift-Voce model [11]. Kim et al. analyzed the numerical modeling accuracy of different AHSS based on the models of Swift, Voce and their combination and obtained the best results for a TRansform Induced Plasticity (TRIP) steel using the combined Swift-Voce model [12].

The HMnS X40MnCrAlV19-2 LY investigated in the present work is classified as AHSS and is also referred to as TWinning Induced Plasticity (TWIP) steel due to the secondary deformation mechanism that dominates during forming. In order to model the flow behavior of TWIP steels for the shearing process during fine blanking, fundamental investigations are still lacking with regard to appropriate extrapolation models as well as thermoviscoplastic models that describe the flow behavior as a function of strain rate and temperature. Therefore, the thermoviscoplastic flow curve model according to Hensel-Spittel was analyzed in this work. For this purpose, flow curves of the HMnS were determined by means of SCT while varying the strain rate and temperature. To extrapolate the single flow curves, the combined Swift-Voce model was compared with the Hockett-Sherby hardening law. The parameters for the thermoviscoplastic Hensel-Spittel model were determined based on a regression analysis using the resulting sets of curves of an extrapolation model for the varied temperature and strain rate range. The Hensel-Spittel model parameters derived from an extrapolated set of curves were then investigated in a FE model for fine blanking and evaluated by means of experimentally determined values of the blanking force as well as sheared surface temperature.

Experimental setup and numerical modeling

The mechanical properties as well as the TWIP effect dominated hardening behavior of hot-rolled HMnS X40MnCrAlV19-2 LY (1.7401) were investigated in the context of fine blanking in a previous work of the authors [2] and are therefore not detailed in the following. The SCTs were carried out on a servo-hydraulic testing machine *Servotest TMTS*, which enables tempered compression tests at high strain rates by means of a closed-loop controlled oven. The upsetting plates were manufactured from ceramic and the surfaces in contact with the specimens were ground and polished. The SCTs were conducted with an aspect ratio of h/d = 1.5 to minimize the influence of friction and ensure sufficient stability. The 5.1 mm thick sheet metal specimens were water jet cut with material allowance, stacked in three layers considering the rolling direction and then finish-turned to a diameter of d = 10.2 mm for achieving sufficient dimensional and shape accuracy. Due to complicated handling for positioning and aligning the stacked specimens in the oven, the SCTs were carried out without lubricant on the contact surfaces to the upsetting plates. To ensure stacked alignment, the samples were fixed with thin tape before positioning.

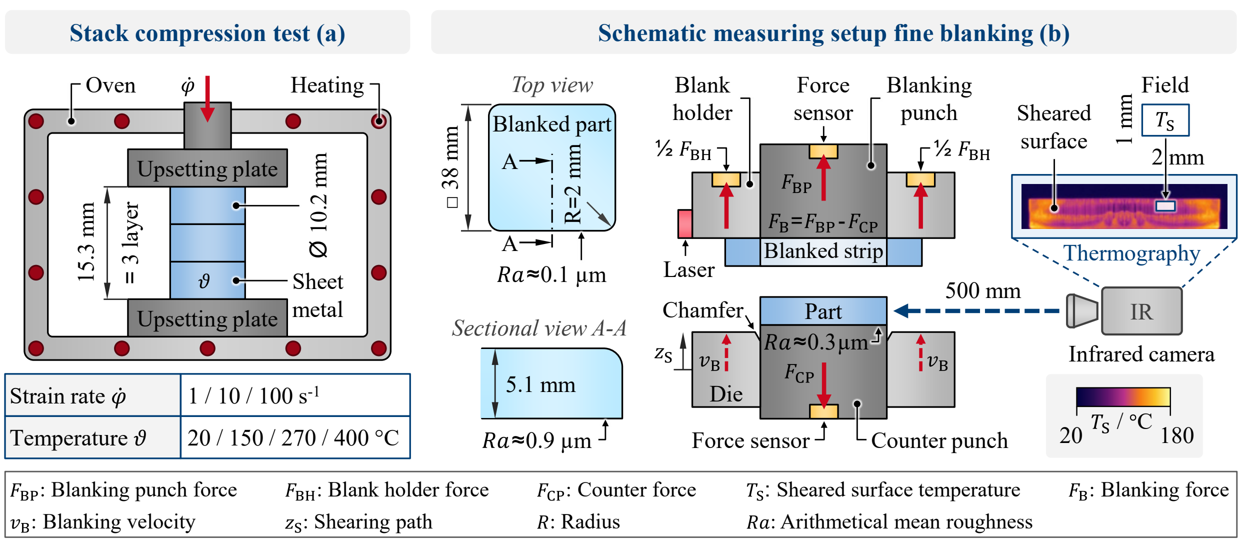

Figure 1 – Setup for stack compression tests (a) as well as thermomechanical measuring setup for fine blanking (b)

Fig. 1a shows the experimental setup as well as the parameters of temperature ϑ and strain rate $\dot{\varphi}$ investigated in the SCT full factorial. Three test repetitions were conducted for each parameter combination. For the flow stresses σ_{SCT} determined in the SCT, the influence of friction was corrected based on the friction hill analysis (e.g. [3]) according to Eq 1. The corrected flow stress σ_{fh} results from the currently measured height h and the radius r as well as the coefficient of friction μ, whereby the radius is calculated from the height assuming volume constancy during the upsetting process. Since no friction coefficients have yet been determined for the investigated test conditions, a constant Coulomb friction with values of $\mu_1 = 0.06$ as well as $\mu_2 = 0.1$ were considered as a first approach. The corrected flow curves were then extrapolated using the combined Swift-Voce model (e.g. [11]) according to Eq. 2 as well as the Hockett-Sherby hardening law [13] according to Eq. 3 up to a true strain of $\varphi = 2.5$ in each case. The corresponding parameters β, A_i, B_i, C_i and n_i as well as those for the Hensel-Spittel model (Eq. 4) were each determined using a non-linear regression analysis in Python based on the method of least squares.

$$\sigma_{\mathrm{fh}} = 2 \cdot \sigma_{\mathrm{SCT}} \cdot \alpha^2 \cdot [e^{2 \cdot \alpha} - 2 \cdot \alpha - 1]^{-1} \quad \text{with } \alpha = \mu \cdot r \cdot h^{-1} \tag{1}$$

$$\sigma_{\mathrm{SV}}(\varphi) = (1-\beta) \cdot A_1 \cdot (B_1 + \varphi)^{n_1} + \beta \cdot [A_2 + B_2 \cdot (1 - e^{-C_2 \cdot \varphi})] \tag{2}$$

$$\sigma_{\mathrm{HS}}(\varphi) = A_3 + B_3 \cdot \left(1 - e^{-C_3 \cdot \varphi^{n_3}}\right) \tag{3}$$

$$\sigma_{\mathrm{f}}(\varphi, \vartheta, \dot{\varphi}) = \sigma_0 \cdot e^{m_1 \cdot \vartheta} \cdot \varphi^{m_2} \cdot e^{\frac{m_4}{\varphi}} \cdot \vartheta^{m_8} \cdot (1+\varphi)^{m_5 \cdot \vartheta} \cdot e^{m_6 \cdot \varphi} \cdot \dot{\varphi}^{m_3 + m_7 \cdot \vartheta} \tag{4}$$

The parameters σ_0 and m_1 to m_8 for the thermoviscoplastic flow curve model according to Hensel-Spittel [14] were finally derived from the three different extrapolated flow curve sets of the investigated temperature and strain rate range. The fine blanking tests were carried out on a tool instrumented with force and displacement sensors using the quadratic blanked part geometry shown in Fig. 1b without the use of a vee-ring on the die or blank holder. The sheared surface temperature T_{S} was determined based on thermographic measurements using a 1 x 2 mm^2 measuring field below the blanked edge on the burr side. For the experimental fine blanking tests, five repetitions were carried out with the process and tool parameters specified in Table 1 for averaging the results. The methodical approach for determining the sheared surface temperature, the procedure and boundary conditions for carrying out the fine blanking tests as well as the basic design of the FE process model are described in detail in a previous work of the authors [15].

Table 1 – Applied fine blanking process as well as tool parameters

Blank holder force F_{BH}	560 kN	Blanking velocity v_{B}	45 mm/s	Die chamfer angle	35°
Counter force F_{CP}	145 kN	Die clearance	20 µm	Die chamfer height	0.35 mm

Analogous to the setup used for the fine blanking tests, a 3D FE model was designed using the blanked part symmetry in the Forge NxT 4.0 software. Based on a mesh convergence analysis, all elements in the shear zone were meshed in a circumferential partition (spatial area with defined element size) with a minimum edge length of l_{E} = 0.25 mm as tetrahedral elements. The meshing in the two adjacent partitions was increased by a factor of two in both directions. The elements in the outer remaining partitions were meshed with a minimum edge length of l_{E} = 1.5 mm (Fig. 2a).

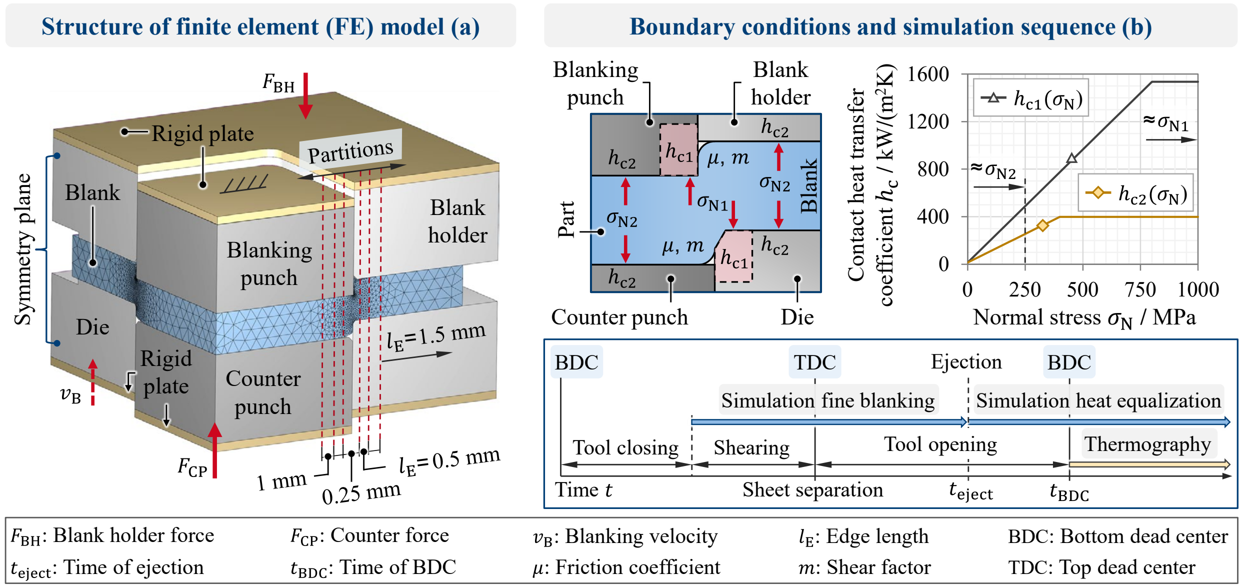

Figure 2 – Structure of FE model (a) with boundary conditions and assignment of the simulation sequence (b)

The friction between the sheet metal material and the tool elements was modeled with a friction coefficient of $\mu = 0.1$ and a shear factor of $m = 0.2$ using a Coulomb friction law limited by the shear friction law. In order to take into account the influence of high contact normal stresses on the contact heat transfer during the shearing process, the contact area was partitioned at the die as well as punch edges. Based on the work of Rosochowska et al. [16], supporting points were derived for the roughness measured on the contact surfaces (cf. Fig. 1) to approximate the contact heat transfer as a linear function depending on the contact normal stress σ_N. Considering the occurring contact normal stresses, the function $h_{c1}(\sigma_N)$ with a high gradient was implemented for the die as well as punch edges and the function $h_{c2}(\sigma_N)$ with a lower gradient was implemented for the remaining area to calculate the contact heat transfer coefficient. From the maximum values shown in the diagram in Fig. 2b, a constant value is assumed for the contact heat transfer. For heat exchange with the environment, a convective heat transfer between air and steel was modeled with a value of h_{conv} = 10 W/(m²·K) and a value of ε_r = 0.21 was used for thermal radiation. All tool elements were elastically modeled to realize a thermally coupled material behavior. The physical and thermophysical parameters for the die and blanking punch (high-speed steel Böhler S390) as well as blank holder and counter punch (cold work steel X155CrVMo12-1 or 1.2379) were modeled temperature-dependent (Table 2) based on a work by Richter et al. [17]. The temperature change of the parameters for the high-speed steel Böhler S390 was derived approximately based on available values for 20 °C using the parameters of the material X54WMoCrV7-5-4-2.

Table 2 – Temperature-dependent parameters used for the Young's modulus E, Poisson's ratio ν; density ρ, thermal conductivity λ, specific heat capacity c and coefficient of thermal expansion α_{th} regarding the tool elements

ϑ [°C]	E [GPa]		ν [-]		ρ [kg/m³]		λ [W/m·K]		c [J/(kg·K)]		α_{th} [10⁻⁶/K]	
Steel	S390	1.2379	S390	1.2379	S390	1.2379	S390	1.2379	S390	1.2379	S390	1.2379
20	231	218	0.303	0.285	8100	7680	17	29.2	420	465	9.4	10.1
100	227	213	0.309	0.287	8078	7660	18.6	30.3	439	483	10	10.7
200	221	206	0.315	0.29	8049	7633	19.4	30.7	459	503	10.5	11.3
300	214	198	0.319	0.294	8018	7604	19.5	29.9	476	520	10.8	11.8
400	206	190	0.322	0.299	7985	7574	19.1	28.8	498	540	11.2	12.2

Materials Research Proceedings 54 (2025) 1856-1867 https://doi.org/10.21741/9781644903599-199

The modeling of the flow behavior for the sheet metal material was carried out thermoviscoplastically according to Eq. 4 using a remeshing algorithm and is discussed in the results section. The temperature-dependent physical and thermophysical parameters specified for the investigated HMnS in Table 3 were derived approximately on the basis of available values for 20 °C using the parameters of the materials X20MnCr24-9 as well as X40MnCr22 [17]. For the consideration of a damage criterion, the modified ductile fracture criterion Cockcroft-Latham normalized by Oh [18] was modeled with a critical fracture threshold value of 1.44 [15].

Table 3 – Temperature-dependent parameters used for the Young's modulus E, Poisson's ratio ν; density ρ, thermal conductivity λ, specific heat capacity c and coefficient of thermal expansion α_{th} regarding X40MnCrAlV19-2 LY

ϑ [°C]	E [GPa]	ν [-]	ρ [kg/m^3]	λ [W/m·K]	c [J/(kg·K)]	α_{th} [10^{-6}/K]
20	192	0.271	7750	12.4	625	14
100	199	0.266	7730	14.9	520	17.1
200	191	0.274	7689	17	522	20
300	182	0.282	7640	18.5	537	21.9
400	172	0.29	7587	19.8	554	23.3

Result analysis

The results of the three test repetitions of the parameter combinations investigated by means of SCT each showed only slight differences in the flow stress progression and were therefore averaged. Fig. 3a shows the temperature influence on the averaged flow stress curves σ_{SCT} at the medium strain rate $\dot{\varphi}$ = 10/s as well as exemplary the correction of the friction influence σ_{fh} calculated according to Eq. 1 for an assumed value of μ_1 = 0.06 as friction coefficient. As generally to be expected, the flow stresses decrease with increasing temperature ϑ, whereby the highest reduction is observed between room temperature (RT) and 150 °C for all three strain rates. With increasing temperature at ϑ = 270 and 400 °C, the maximum true strain φ achieved with the SCT decreases for all investigated strain rates. Fig. 3b shows the influence of the strain rate on the averaged flow stress curves. Starting from RT to ϑ = 270 °C (the latter not shown for a better overview), a higher strain rate of $\dot{\varphi}$ = 100/s initially leads to an increase of the flow stress progression. However, with increasing true strain, the progression of the flow stress falls below the values determined at a low strain rate ($\dot{\varphi}$ = 1/s), whereby the intersection of the curve pairs is shifted to lower true strains with rising temperature. In contrast, a comparable progression between low and high strain rate can be observed for ϑ = 400 °C at the start of forming, whereby a high strain rate leads to an increase in flow stress with increasing true strain. An increase in the strain rate generally causes a dynamically induced flow stress increase of the investigated HMnS, which, however, is superimposed by a softening effect below 400 °C as forming progresses. The observed softening at higher strain rates is due to a significant rise in temperature with increasing forming as a result of activated deformation mechanisms of the HMnS [2].

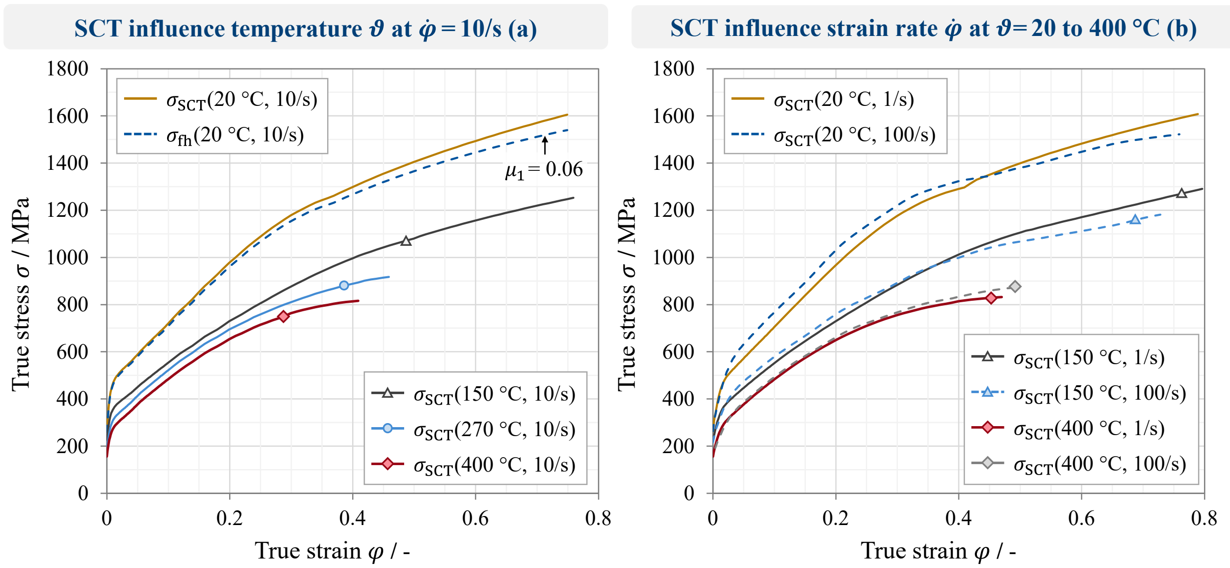

Figure 3 – Temperature (a) and strain rate influence (b) on flow stress progression of HMnS X40MnCrAlV19-2 LY

The flow stress curves determined with the SCT were corrected according to Eq. 1 for assumed friction coefficients of $\mu_1 = 0.06$ (L) as well as $\mu_2 = 0.1$ (H) and subsequently extrapolated to derive the parameters of the Hensel-Spittel flow curve model (Eq. 4) using the Swift-Voce (Eq. 2) and Hockett-Sherby (Eq. 3) models. Both models used for extrapolation map the experimentally determined flow stresses with a coefficient of determination of $R^2 \approx 0.996$ to 0.999 with sufficient accuracy. The weighting factor for the combined Swift-Voce model lies between values of $\beta \approx 0.407$ and 0.851 regarding the investigated temperature and strain rate range. Fig. 4a and b exemplarily show the corrected and extrapolated flow stresses according to Swift-Voce as well as Hockett-Sherby with $\mu_1 = 0.06$ compared to the corresponding derived Hensel-Spittel modeling for RT and 400 °C at medium strain rate. For the combined Swift-Voce model, the flow stresses σ_{SV} increase with increasing true strain. The derived Hensel-Spittel model $\sigma_f\{SV\text{-}L\}$ basically shows a sufficiently accurate mapping of the extrapolated flow curves with $R^2 \approx 0.992$ and differs with a maximum of 50 to 75 MPa. For the Hockett-Sherby hardening law, the flow stress curve σ_{HS} converges towards a limit value with increasing true strain, which leads to lower stress values from a true strain of $\varphi \approx 1.5$ compared to σ_{SV}. The Hensel-Spittel modeling $\sigma_f\{HS\text{-}L\}$ derived from this also maps the underlying extrapolated flow curves with $R^2 \approx 0.984$ with sufficient accuracy and shows similar deviating maximum stresses to the extrapolated progression as for $\sigma_f\{SV\text{-}L\}$.

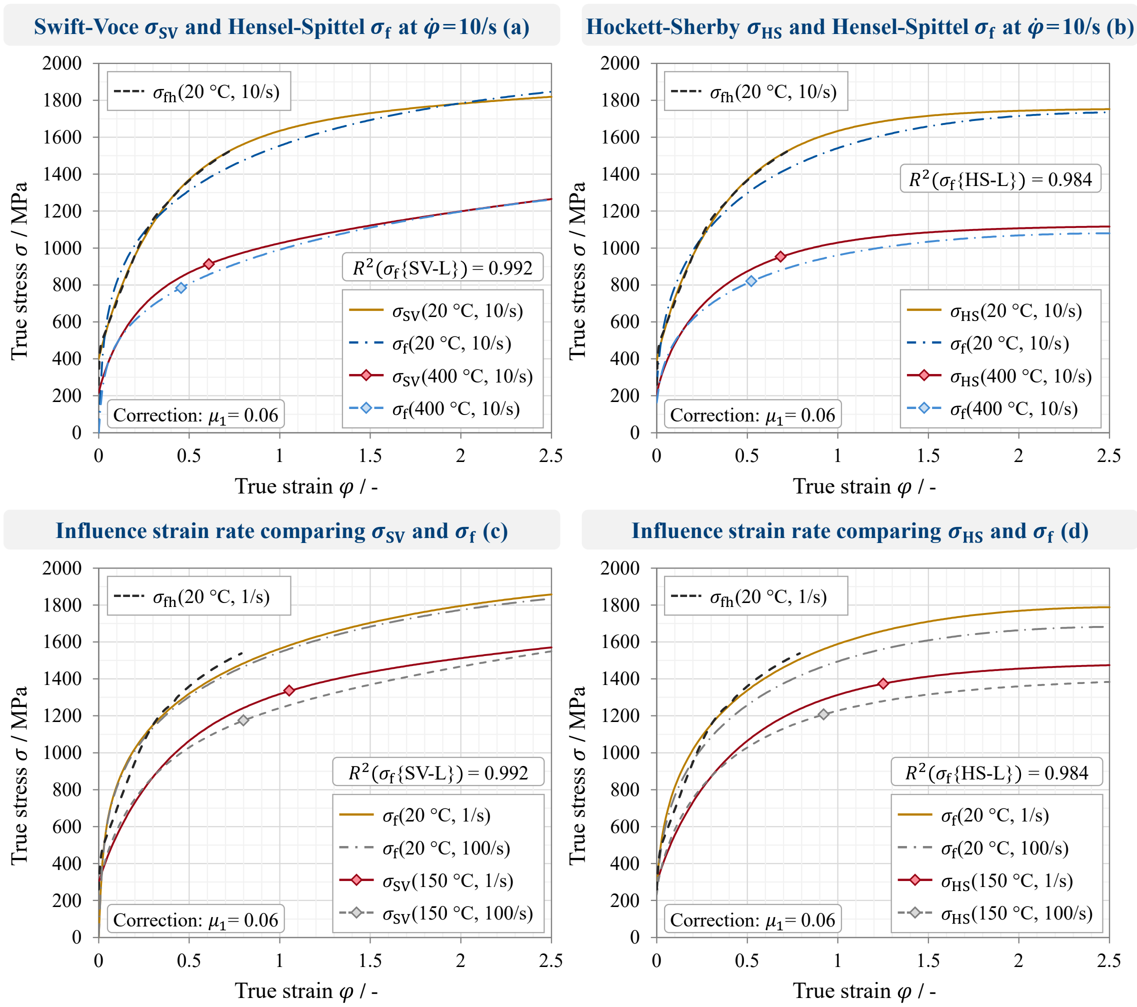

Figure 4 – Comparison of Hensel-Spittel modeling with extrapolation as a function of the temperature for Swift-Voce (a) and Hockett-Sherby (b) as well as the strain rate for Swift-Voce (c) and Hockett-Sherby (d)

Fig. 4c and d exemplarily show the modeling accuracy regarding the influence of low and high strain rate on the flow stress progression for the extrapolation according to Swift-Voce as well as Hockett-Sherby in comparison to the Hensel-Spittel model. Both the Swift-Voce and Hockett-Sherby models map the dynamically induced flow stress increase at the beginning as well as the softening with increasing true strain when the strain rate is raised. In the case of the Swift-Voce extrapolation, the flow stress curve σ_{SV} with a higher strain rate increases more steeply with increasing true strain than with a lower one, as a result of which both curves approach each other. In contrast, the extrapolated flow stresses for the Hockett-Sherby model σ_{HS} show an approximately parallel curve for high and low strain rates with increasing true strain.

The Hensel-Spittel modeling does not map the dynamically induced flow stress increase at the beginning of the stress progression. The Hensel-Spittel curves $\sigma_f\{\text{SV-L}\}$ based on the Swift-Voce extrapolation show a smaller and parallel softening compared to σ_{SV} at high strain rate and increasing true strain. The Hensel-Spittel curve $\sigma_f\{\text{HS-L}\}$ derived from the extrapolation according to Hockett-Sherby is mapped in terms of the high strain rate with a softening comparable to σ_{HS}. The characteristics shown in Fig. 4 are transferable to the flow stresses corrected and extrapolated with $\mu_2 = 0.1$ as well as the Hensel-Spittel modeling $\sigma_f\{\text{SV-H}\}$ derived from them. Table 4 shows the Hensel-Spittel model parameters determined for the numerical analysis.

Table 4 – Derived parameters for the Hensel-Spittel flow curve modeling according to Eq. 4

Model	σ_0 [MPa]	m_1 [10^{-3}]	m_2 [10^{-1}]	m_3 [10^{-3}]	m_4 [10^{-3}]	m_5 [10^{-4}]	m_6 [10^{-1}]	m_7 [10^{-5}]	m_8 [10^{-2}]
SV-H	1890.39	-1.04149	2.56425	-0.79725	-8.19896	3.6981	-0.59551	0.186	-4.73631
SV-L	1902.7	-1.11935	2.72698	-2.77314	-6.91179	3.279	-0.56882	0.481	-3.83129
HS-L	1978.14	-1.0949	3.43192	-13.5856	0.46493	-0.0602	-1.3053	1.431	-2.24016

Fig. 5a compares the blanking force curve F_B(HMnS Exp) averaged from the experimental fine blanking tests with the numerically determined curves $F_B(\sigma_f)$. Compared to the experimental result, the numerically determined blanking force curves show a qualitatively comparable progression, which, however, slightly deviates towards the end of the shearing process. The Hensel-Spittel modeling based on σ_{SV} with a lower friction correction σ_f\{SV-L\} is with a maximum blanking force of 476.1 kN slightly below the experimentally determined value and proceeds above the other numerical force curves with increasing shearing path ($z_S \approx 2.2$ mm). The Hensel-Spittel modeling σ_f\{SV-H\} based on the higher friction correction results in the lowest maximum blanking force of 463.6 kN. The Hensel-Spittel modeling σ_f\{HS-L\} derived from σ_{HS} with a lower friction correction leads to a slightly higher maximum blanking force of 490.5 kN compared to the experimental result. However, with increasing shearing path, the blanking force progression of $F_B(\sigma_f$\{HS-L\}) falls below the other numerically determined force curves.

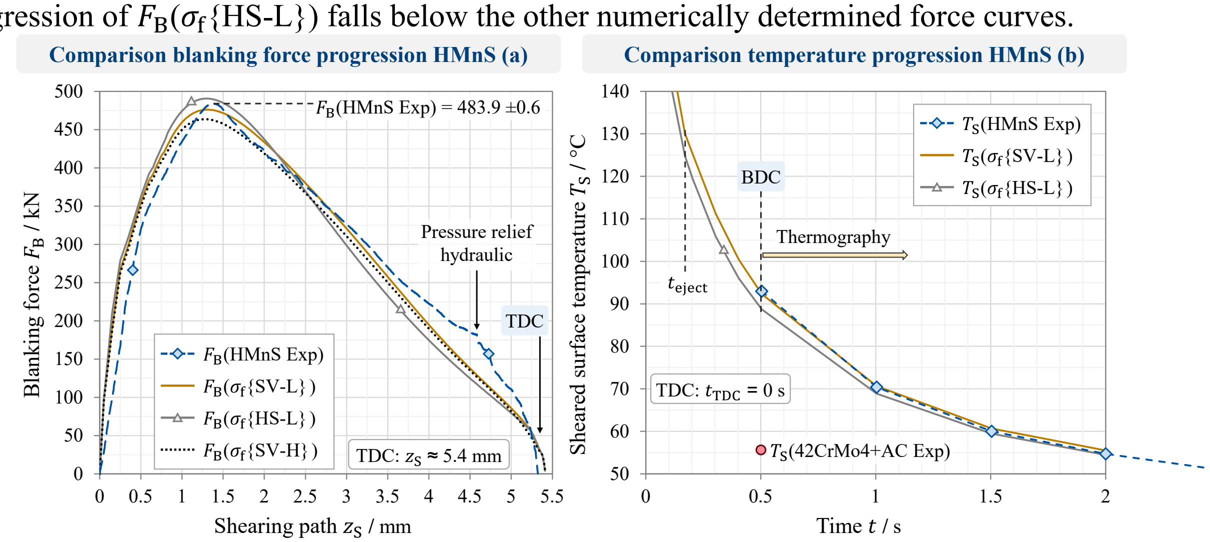

Figure 5 – Comparison of the determined blanking force (a) as well as temperature curves (b)

Compared to the experimental blanking force, all numerically determined curves rise more steeply at the start of shearing and consequently reach their maxima slightly earlier regarding the shearing path. From a shearing path of $z_S \approx 3.7$ mm, a significantly increasing gradient can be observed in the experimental blanking force curve, which kinks due to a machine-related pressure relief of the hydraulically applied blank holder and counter forces and falls steeply as a result of an abrupt separation. The significant increase in the experimental blanking force before the kink is assumed to be due to process-related friction effects between the active tool elements, which are not modeled numerically. Fig. 5b shows the experimentally and numerically determined progression of the sheared surface temperature T_S, which is based on the averaged values of the measuring field defined in Fig. 1b. The numerically determined sheared surface temperatures fall exponentially after separation of the sheet metal material at top dead center (TDC) and show a qualitatively comparable progression to the thermographically determined values from bottom dead center (BDC). Starting from the BDC, the Hensel-Spittel modeling σ_f\{SV-L\} shows a sufficiently accurate correspondence to the experimentally determined sheared surface temperatures. The temperature progression of the Hensel-Spittel model $T_S(\sigma_f\{\text{HS-L}\})$ derived from σ_{HS} is lower than $T_S(\sigma_f\{\text{SV-L}\})$, which is particularly reflected in the comparison at the beginning of the thermographic measurements. The Hensel-Spittel modeling $\sigma_f\{\text{SV-H}\}$, which is based on the higher friction correction, overlaps with the progression of the sheared surface temperature $T_S(\sigma_f\{\text{HS-L}\})$ and is only shown quantitatively in Table 5 for a better overview.

Table 5 – Results with standard deviations of sheared surface temperature T_S [°C] starting with t_{eject} = 0.1704 s

Time t [s]	0.1704	0.204	0.304	0.404	0.504	1.004	1.504	2.004
HMnS Exp	---	---	---	---	93 ±1	70.4 ±1.2	60 ±1.2	54.7 ±1.2
$\sigma_f\{\text{SV-L}\}$	130.1 ±2.5	125.2 ±2.1	111.2 ±1.3	100.4 ±1	92.3 ±0.7	70.6 ±0.3	60.7 ±0.1	55.5 ±0.1
$\sigma_f\{\text{HS-L}\}$	124.8 ±2.2	119.4 ±1.8	105.8 ±1.2	96 ±0.9	88.7 ±0.7	68.9 ±0.3	59.5 ±0.1	54.4 ±0.1
$\sigma_f\{\text{SV-H}\}$	124.6 ±2.2	119.8 ±1.9	106.4 ±1.3	96.4 ±0.9	89.7 ±0.7	69.1 ±0.3	59.6 ±0.1	54.6 ±0.1

Discussion and conclusion

For thermoviscoplastic flow curve modeling of the TWIP steel X40MnCrAlV19-2 LY (HMnS), a temperature range of 20 to 400 °C with strain rates of 1 to 100/s was investigated in the SCT. Below 400 °C, the stress curves determined in the SCT at a high strain rate showed a dynamically induced flow stress increase at the beginning of upsetting, which is observable in tensile tests at 20 °C for the entire range of the investigated strain [2]. In the SCT, however, the flow stress increase with increasing true strain is superimposed by a thermally induced softening effect, so that the flow stresses are reduced at temperatures below 400 °C due to the increase in strain rate. The thermal softening of the HMnS observed in the SCT is consistent with reduced sheared surface hardening at increased blanking velocity in a previous work [2] and thus confirms the thermomechanical influence on the activation of the deformation mechanisms during the shearing process in fine blanking. The Hensel-Spittel model derived from the extrapolated sets of flow curves maps the stress progression with increasing true strain with sufficient accuracy and thus the thermal softening at higher strain rates, but not the dynamically induced flow stress increase at the beginning of upsetting. The Hensel-Spittel modeling $\sigma_f\{\text{SV-L}\}$ derived from the Swift-Voce extrapolation showed for the numerically determined blanking force progression as well as subsequent heat equalization at the sheared surface the best correspondence to the experimentally determined results. The Hensel-Spittel modeling $\sigma_f\{\text{HS-L}\}$ based on the Hockett-Sherby extrapolation results in lower flow stresses with increasing true strain and a steeper decrease in the blanking force progression, which is a possible cause for the lower numerical sheared surface temperatures. Fig. 6 summarizes the observed results in context of the underlying approach.

The sheared surface temperature determined experimentally for HMnS at the BDC is approx. 66% (cf. Fig. 5b) higher than the temperature of 42CrMo4+AC (AISI 4140) determined under comparable boundary conditions [15], which shows a significant thermal influence on the shear zone due to the hardening behavior dominated by the TWIP effect. The correlations shown in Fig. 4 and 5 are based on a correction of the flow stress with an assumed value of μ_1 = 0.06 for the friction coefficient. Kraus et al. determined a significantly higher friction coefficient with an average value of μ = 0.136 for the AHSS DP600 with an aspect ratio of h/d = 0.1 for single-layer SCT without lubricant [8]. In further research, an analysis of the friction occurring during the SCT of HMnS is therefore required regarding the aspect ratio of h/d = 1.5 used to reduce the influence of friction on the flow stress. In summary, the following conclusions are derived:

- At temperatures below 400 °C, an increase of the strain rate leads to a dynamically induced flow stress increase at the start of upsetting in the SCT of HMnS X40MnCrAlV19-2 LY. With increasing true strain, this is superimposed by a thermally induced softening effect, which leads to a reduced flow stress compared to a low strain rate.

- The thermoviscoplastic Hensel-Spittel flow curve model only maps the thermally induced softening effect with increasing true strain when the strain rate is increased.
- The Hensel-Spittel model parameters derived from the set of flow curves extrapolated with the combined Swift-Voce model showed the best correspondence to the experimentally determined values regarding the numerical comparison.
- Compared to conventional steels, fine blanking of HMnS leads to a significant increase of the sheared surface temperature due to activated deformation mechanisms during the shearing process.

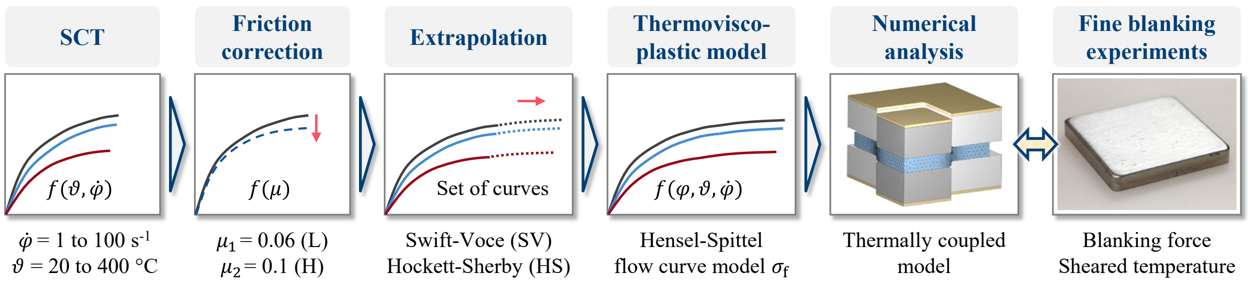

Derived flow curve model	Dynamically induced flow stress increase	Thermally induced softening effect	Maximum blanking force	Blanking force progression	Sheared surface temperature BDC	Sheared surface temperature progression
$\sigma_f(\mu_2, \text{SV})$	Accuracy: Low	Medium	Low	Medium	Medium	Medium
$\sigma_f(\mu_1, \text{SV})$	Accuracy: Low	Medium	Medium	High	High	High
$\sigma_f(\mu_1, \text{HS})$	Accuracy: Low	High	Medium	Low	Medium	Medium

Figure 6 – Summarized evaluation of the modeling accuracy in context of the investigated approach

Acknowledgements
The authors would like to thank the *German Research Foundation (DFG)* for funding this work as part of the project "Fine Blanking Induced Plasticity" under the project number 548386476, the *Institute of Metal Forming IBF of RWTH Aachen University* for carrying out the SCTs as well as *thyssenkrupp Hohenlimburg GmbH* for providing the HMnS.

References

[1] P. Demmel, H. Hoffmann, R. Golle, C. Intra, and W. Volk, Interaction of heat generation and material behaviour in sheet metal blanking, CIRP Annals, vol. 64, no. 1, pp. 249–252, (2015). https://doi.org/10.1016/j.cirp.2015.04.091

[2] S. N. Babaei, F. Schweinshaupt, S. Wipp, T. Herrig, U. Krupp, and T. Bergs, Mechanism-driven fine blanking of high manganese steels, Journal of Materials Processing Technology, vol. 319, p. 118083, (2023). https://doi.org/10.1016/j.jmatprotec.2023.118083

[3] M. Rossi et al., Testing methodologies for the calibration of advanced plasticity models for sheet metals: A review, Strain, vol. 58, no. 6, (2022). https://doi.org/10.1111/str.12426

[4] S. Coppieters, H. Traphöner, F. Stiebert, T. Balan, T. Kuwabara, and A. E. Tekkaya, Large strain flow curve identification for sheet metal, Journal of Materials Processing Technology, vol. 308, p. 117725, (2022). https://doi.org/10.1016/j.jmatprotec.2022.117725

[5] G. E. Dieter, Mechanical metallurgy, SI Metric ed., Boston, Mass.: McGraw-Hill, 1988.

[6] Y. G. An and H. Vegter, Analytical and experimental study of frictional behavior in through-thickness compression test, Journal of Materials Processing Technology, vol. 160, no. 2, pp. 148–155, (2005). https://doi.org/10.1016/j.jmatprotec.2004.05.026

[7] B. Hochholdinger, H. Grass, A. Lipp, and P. Hora, Determination of Flow Curves by Stack Compression Tests and Inverse Analysis for the Simulation of Hot Forming, Proceedings of the 7th European LS-DYNA Conference, pp. 1–11, (2009).

[8] M. Kraus, M. Lenzen, and M. Merklein, Contact pressure-dependent friction characterization by using a single sheet metal compression test, Wear, vol. 476, p. 203679, (2021). https://doi.org/10.1016/j.wear.2021.203679

[9] M. L. Kölüs, R. Borbély, and G. J. Béres, The effect of friction compensation on the slope of flow curves obtained by stack compression tests, Materials Research Proceedings, Vol. 41, pp 1182-1189, (2024). https://doi.org/10.21741/9781644903131-131

[10] M.-S. Joun, M. K. Razali, C.-W. Jee, J.-B. Byun, M.-C. Kim, and K.-M. Kim, A Review of Flow Characterization of Metallic Materials in the Cold Forming Temperature Range and Its Major Issues, Materials, vol. 15, no. 8, (2022). https://doi.org/10.3390/ma15082751

[11] X. Lemoine, S. Sriram, and R. Kergen, Flow Curve Determination at Large Plastic Strain Levels to Accurately Constitutive Equations of AHSS in Forming Simulation, in: AIP Conf. Proc., pp. 1417–1422, (2011). https://doi.org/10.1063/1.3589715

[12] S. Kim, J. Lee, F. Barlat, and M.-G. Lee, Formability prediction of advanced high strength steels using constitutive models characterized by uniaxial and biaxial experiments, Journal of Materials Processing Technology, vol. 213, no. 11, pp. 1929–1942, (2013). https://doi.org/10.1016/j.jmatprotec.2013.05.015

[13] J. E. Hockett and O. D. Sherby, Large strain deformation of polycrystalline metals at low homologous temperatures, Journal of the Mechanics and Physics of Solids, vol. 23, no. 2, pp. 87–98, (1975). https://doi.org/10.1016/0022-5096(75)90018-6

[14] A. Hensel and T. Spittel, Kraft- und Arbeitsbedarf bildsamer Formgebungsverfahren: Mit 51 Tabellen, 1st ed. Leipzig: Dt. Verl. für Grundstoffindustrie, 1978.

[15] F. Schweinshaupt, T. Stoel, M. Müller, T. Herrig, and T. Bergs, Thermomechanical modeling of the shearing process during fine blanking of quenched and tempered steel, Procedia Structural Integrity, vol. 61, pp. 214–223, (2024). https://doi.org/10.1016/j.prostr.2024.06.028

[16] M. Rosochowska, R. Balendra, and K. Chodnikiewicz, Measurements of thermal contact conductance, Journal of Materials Processing Technology, vol. 135, 2-3, pp. 204–210, (2003). https://doi.org/10.1016/S0924-0136(02)00897-X

[17] F. Richter, Die physikalischen Eigenschaften der Stähle - Das 100-Stähle-Programm, available: https://www.tugraz.at/fileadmin/user_upload/Institute/IEP/Thermophysics_Group /Files/Staehle-Richter.pdf (accessed: Jan. 2, 2025).

[18] S. I. Oh, C. C. Chen, and S. Kobayashi, Ductile Fracture in Axisymmetric Extrusion and Drawing – Part 2: Workability in Extrusion and Drawing, Journal of Engineering for Industry, vol. 101, no. 1, pp. 36–44, (1979). https://doi.org/10.1115/1.3439471